Importance of Active Site 'Canopy' Residues in an O_2-tolerant [NiFe]-hydrogenase

Emily J. Brooke,[1] Rhiannon M. Evans,[1] Shams T. A. Islam,[1] Gerri M. Roberts,[2]

Sara A. M. Wehlin,[1] Stephen B. Carr[3,4], Simon E. V. Phillips[3,4] and Fraser A. Armstrong[1]

[1]Department of Chemistry, University of Oxford, Oxford, UK. [2]Division of Chemistry and Chemical Engineering, California Institute of Technology, Pasadena, California 91125. [3]Research Complex at Harwell, Rutherford Appleton Laboratory, Harwell Oxford, Didcot, UK. [4]Department of Biochemistry, University of Oxford, Oxford, UK.

Supplementary Information

Contents

Sequence Alignment

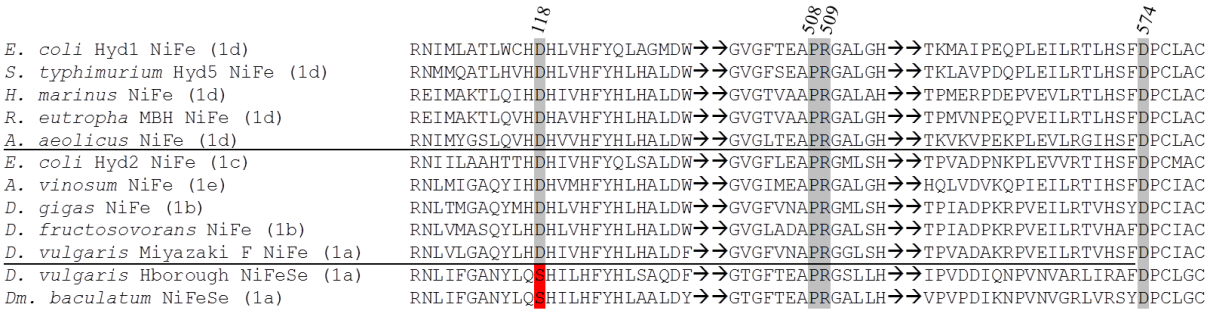

Figure S1: Selected sequence alignment. The large subunit regions of various O_2-tolerant (Group 1d, top), and O_2-sensitive (various subgroups as indicated, middle) [NiFe]-hydrogenase and [NiFeSe]-hydrogenases (Group 1a, bottom) are shown. Canopy residues 118, 508, 509 and 574 are highlighted in grey and the Asp-to-Ser substitution at position 118 is highlighted for the [NiFeSe]-hydrogenases in red. *E. coli* Hyd-1 numbering is used. Note that the 576 cys is Se-cys in [NiFeSe]-hydrogenases. A more comprehensive sequence alignment has been summarized in Table S1. Sequence alignment adapted from reference (*1*)

Table S1: Variation in canopy residues across the [NiFe]-hydrogenase subgroups. A detailed analysis of the possible amino acids in positions equivalent to E28, D118, P508, R509 and D574 across all different groups of [NiFe] –hydrogenases based on an extended sequence alignment. The (meta)genomic analysis from Greening et al., was used as a sequence database and includes sequences of putative hydrogenases classified according to metal binding motifs and genome/domain organization.(*2*)

[NiFe(Se)] groups aligned against Group 1 to identify Hyd-1 canopy equivalent residues	**Group 1 – Membrane bound H_2 uptake:** • 1A = Ancestral – includes NiFeSe (sulfate, organohalide, methanogenic and heterodisufide respiration) • 1B = Prototypical (sulfate, fumarate, nitrate respiration) • 1C = Hyb type (includes *E.coli* Hyd2) – fumarate reduction, possibly bidirectional • 1D = O_2 tolerant (includes *E.coli* Hyd-1) – aerobic respiration and O_2 tolerant anaerobic respiration • 1E = Isp type – sulfur respiration, possibly bidirectional • 1F = unresolved – may be linked to reduction of reactive oxygen species • 1G = unresolved – may be linked to sulfur respiration • 1H/5 = Tropospheric H_2 scavenging in aerobic respiration/starvation	**Group 2 – Cytosolic H_2 uptake:** • 2A = Cyanobacteria type –aerobic respiration, H_2 recycling (from nitrogenase, fermentation) • 2B = HK linked – Senses H_2 and activates two-component cascade controlling H_2ase expression • 2C = DGC linked (putative) – predicted to sense H_2 and induce cyclic di-GMP production • 2D = Aquificae type – unknown. May generate reductant for C fixation	**Group 3 – cytosolic bidirectional:** • 3A = F_{420} coupled – Directly couples oxidation of H_2 to reduction of F_{420} during methanogenesis. Reverse reaction may also occur. Includes [NiFeSe] variants • 3B: NADP coupled - Directly couples oxidation of NADPH to evolution of H_2. May be reversible. Some complexes are proposed to have sulfhydrogenase activity • 3C: HDR linked – Bifurcates electrons from H_2 to heterodisulfide and ferredoxin in methanogens without cytochromes • 3D: NAD coupled – Directly interconverts electrons between H_2 and NAD depending on redox state	**Group 4 – Membrane bound H_2 evolving:** • 4A = FHL type – Couples oxidation of formate to fermentative H_2. Hyf-type complexes may translocate H^+ via antiporter modules • 4B = Mrp linked – Couples oxidation of HCO_2 or CO to proton reduction. Generates Na-motive force via Mrp antiporter modules • 4C = CODH linked – Forms complex with CODH to anaerobically respire CO using H^+ as terminal e^- acceptors. • 4D = Eha/Ehb type – Multimeric, H_2 oxidation/ferredoxin reduction for anaplerotic (Eha) and anabolic (Ehb) purposes. H^+/Na^+ driven • Group 4e: Ech type – Couples ferredoxin oxidation to H_2 evolution. This process is physiologically reversible via H^+/Na^+ translocation • Group 4f: Ehf type (putative) – Unknown. May couple oxidation of a one-carbon compound to proton reduction concurrent with proton translocation. Related to Ehr complexes.
Number of sequences identified	781	207	549	461

E28 conservation	DEPENDS ON SUBGROUP: ○ 1A = E N S G H ○ 1B = E ○ 1C = E ○ 1D = E ○ 1E = E ○ 1F = E ○ 1G = A E ○ 1H/5 = V I	Strictly conserved	DEPENDS ON SUBGROUP: ○ 3A = E S A ○ 3B = E ○ 3C = E ○ 3D = E	Strictly conserved
D118 conservation	DEPENDS ON SUBGROUP: ○ 1A = S D N ○ 1B =D ○ 1C = D ○ 1D = D ○ 1E = D ○ 1F = D ○ 1G = D ○ 1H/5 = D	DEPENDS ON SUBGROUP: ○ 2A = S N D ○ 2B = D S ○ 2C = S N ○ 2D = N S	DEPENDS ON SUBGROUP: ○ 3A = N S D V ○ 3B = S N D ○ 3C = D E S ○ 3D = S	DEPENDS ON SUBGROUP: ○ 4A = S ○ 4B = S N ○ 4C = S ○ 4D = S ○ 4E = S ○ 4F = N
P508 conservation	DEPENDS ON SUBGROUP: ○ 1A =P A S M G T I V ○ 1B = P A T ○ 1C =P S ○ 1D =P ○ 1E = P ○ 1F =P A S ○ 1G =P G ○ 1H/5 = V	DEPENDS ON SUBGROUP: ○ 2A = A I S M ○ 2B = A ○ 2C =A P V ○ 2D = A S T C P	DEPENDS ON SUBGROUP: ○ 3A = P A ○ 3B = P A ○ 3C = P N A T S ○ 3D = P	DEPENDS ON SUBGROUP: ○ 4A = P ○ 4B =P H ○ 4C =P ○ 4D =P Q H ○ 4E =P S ○ 4F =P A
R509 conservation	CONSERVED R/K: Only one incidence of arginine substitution in case of *Clostridium clariflavum* (Group 1a). Sequence comparison of *C. clariflavum* and *E. coli* Hyd-1 shows 26.8% identity (53.9% similarity) in a 568 amino acid overlap region	Strictly conserved R	Strictly conserved R	Strictly conserved R
D574 conservation	Strictly Conserved	Strictly Conserved	Strictly conserved	D in all subgroups except 4F where is conservatively substituted for E

Table S2: Oligonucleotide primers, plasmid constructs and *E. coli* strains for P508A variant enzyme production

Plasmid Name	**Plasmid Function**	
pMAK-hyaB-P508A	Mutated plasmid for transfer of codon change to FTH004 chromosome to create P508A variant strain	
Primer name	**Primer function**	**Primer Sequence**
hyaB_P508A_F	*hyaB* P508A mutagenesis forwards primer	5'-GGT TTT ACC GAA GCG GCC CGC GGG GCG TTA GGC CAC TGG-3'
hyaB_P508A_R	*hyaB* P508A mutagenesis reverse primer	5'-CCA GTG GCC TAA CGC CCC GCG GGC CGC TTC GGT AAA ACC-3'
Strain name	**Strain description**	
STAI01	P508A variant strain. Strain produced by codon change on chromosome of FTH004 strain using *pMAK-hyaB*-P508A plasmid	

Denaturing electrophoresis

P508A was indistinguishable from native Hyd-1 by denaturing electrophoresis, comprising large subunit (HyaB) and His-tagged small subunit ($HyaA^{His}$), with both being proteolytically-processed correctly.

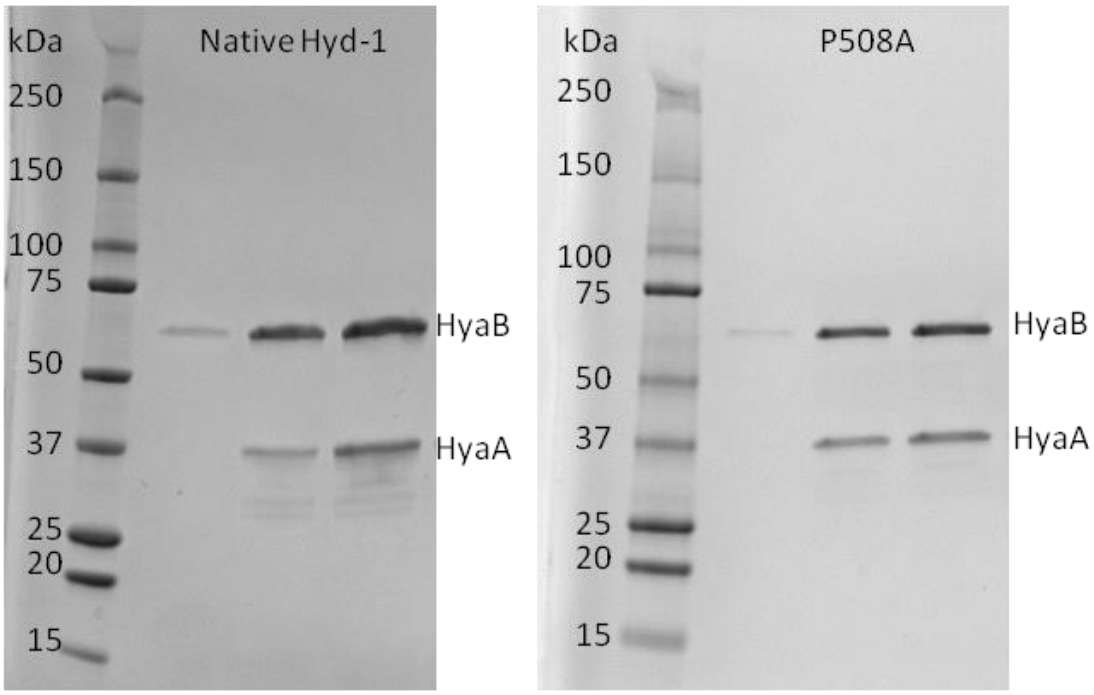

Figure S2: Denaturing (SDS) polyacrylamide gel electrophoresis of native Hyd-1 and P508A. Each enzyme is loaded following Ni-affinity, size exclusion and hydroxyapetite purification as described previously.(*1*) Protein bands corresponding to the mass expected for the large (HyaB) and small (HyaA) subunit are indicated.

Table S3: X-ray data collection and refinement statistics for Hyd-1 P508A

Crystal parameters[a]	
Space group	$P2_12_12_1$
Cell dimensions (Å)	a = 94.68, b = 98.59, c = 185.35
Resolution (Å)	98.59–1.2 (1.22–1.2)
Total reflections	3,867,154 (184,036)
Unique reflections	536,585 (26,248)
Completeness	100 (99.5)
Multiplicity	7.2 (7.0)
$\langle I/\sigma \rangle$	7.3 (1.6)
R_{merge}[b]	11.3 (136)
R_{pim}[c]	4.8 (58.3)
$CC_{1/2}$	0.995 (0.65)
Refinement R_{work}/R_{free}[d]	12.1/14.1
Model	
Protein atoms	13646
Metal ions	28
Waters	1408
RMSD bond lengths (Å)	0.019
RMSD angles (°)	1.90
Ramachandran plot (%)	favored 96.7; outliers 0.

a values in parenthesis refer to highest resolution shell. *b* $R_{merge} = \Sigma_{hkl}\Sigma_i|I_i(hkl)-\langle I_i(hkl)\rangle|/\Sigma_{hkl}\Sigma I_i(hkl)$, where $I_i(hkl)$ is the intensity of reflection hkl and Σ_i is the sum over all i measurements of reflection hkl. *c* $R_{pim}=\Sigma_{hkl}(1/N-1)^{1/2}\ \Sigma_i|I_i(hkl) - \langle I(hkl)\rangle|/\ \Sigma_{hkl}\Sigma_i I_i(hkl)$ where I is the integrated intensity of a given reflection and $\langle I \rangle$ is the mean intensity of multiple corresponding, symmetry related reflections and N is the multiplicity of a given reflection. *d* $R_{work} = \Sigma_{hkl}||F_{obs}|-F_{calc}||/\Sigma_{hkl}|F_{obs}|$ where F_{obs} and F_{calc} are the observed and calculated structure factors respectively. R_{free} is calculated in the same manner, but using a random subset (5%) of reflections that are excluded from refinement.

Structure of P508A

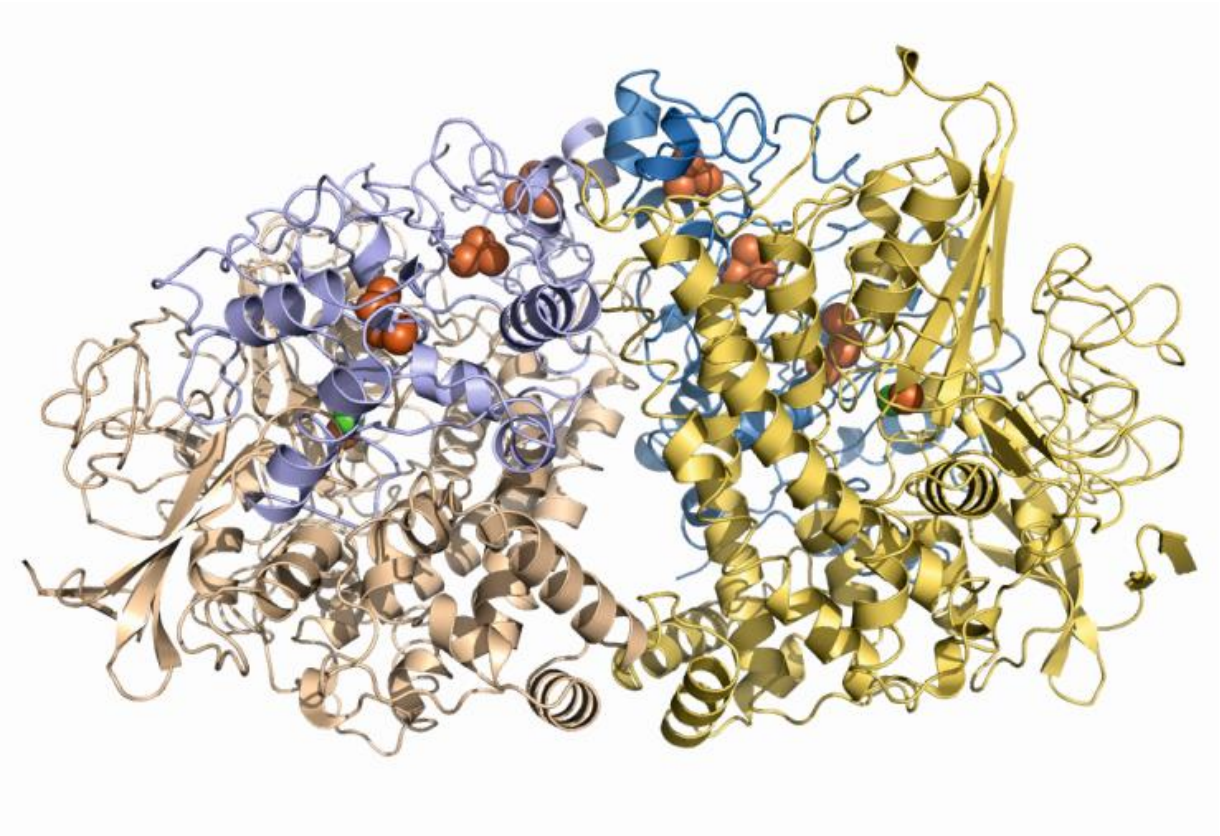

Figure S3: Overall Structure of P508A. Overall structure of Hyd-1 P508A shows no significant changes to the protein structure when compared to native enzyme (polypeptide backbones can be superposed with an rmsd of 0.47 Å). The small subunit chains are colored blue and purple, and the large subunits gold and fawn. The FeS clusters and [NiFe] center are shown as spheres.

Table S4: Average temperature factors for residues at the catalytic center of variants. All values calculated using Baverage from the CCP4 suite of programs. Only variant structures of similar resolution are compared.

Residue	**P508A**	**D574N**	**D118A**	**D118N/D574N**
Resolution/Å	1.2	1.23	1.25	1.1
118	16.3	10.8	8.9	7.7
508	11.7	8.4	8.7	7.6
509	13.5	9.0	14.0	9.6
574	14.3	9.8	11.1	8.2

Overlay of native Hyd-1 and P508A

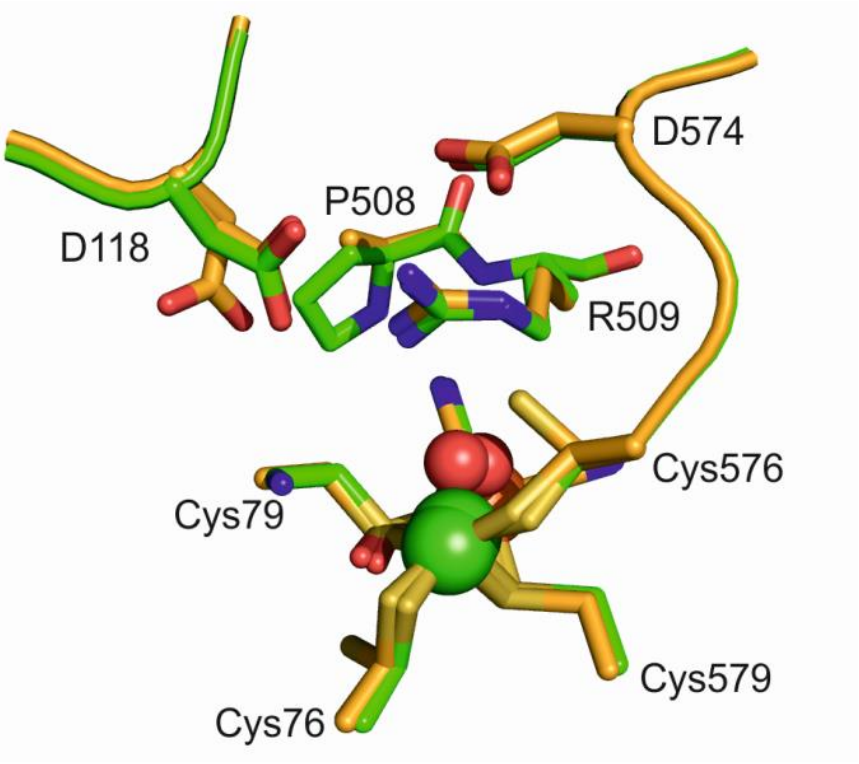

Figure S4: Overlay of the [NiFe] center of native Hyd-1 and the P508A variant. The carbon atoms of native Hyd-1 are colored green whilst those of P508A are colored orange. The Ni and Fe ions are shown as turquoise and bronze spheres respectively and the bridging hydroxide is represented as a red sphere. Residue C79 is modeled as sulfenic acid due to oxidation of the sulfur atom of this amino acid. Multiple conformations can be observed for the side chains of terminal cysteine residues C76 and C576. Occupancy refinement of the two conformations of C76/576 suggests 80% of side chains are in the coordinating position. The occupancy of the Ni ion was also found to be approximately 80%.

Alternate Conformations of D118 in the P508A variant

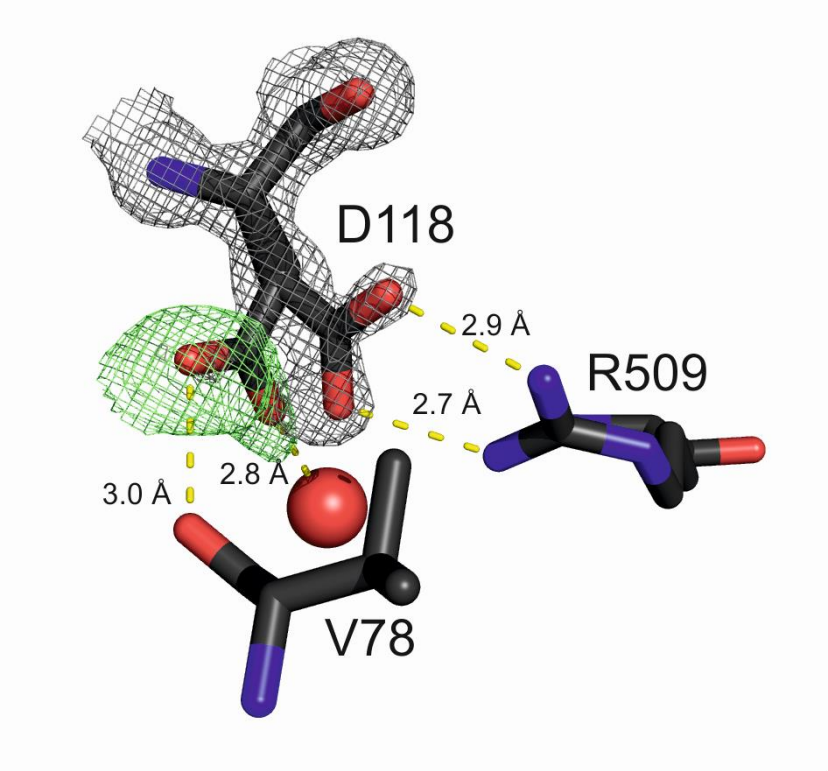

Figure S5: Side chains conformations of D118 and R509 in Hyd-1 variant P508A. 2Fo-Fc electron density maps (grey) show D118 forms a salt bridge with R509, however, Fo-Fc positive difference density maps (green) indicate the side chain can adopt a second distinct conformation. The relative occupancies of the two conformers show approximately 80% maintain an interaction with R509 while 20% do not. The extra water molecule observed at the active site in the P508A variant is shown as a red sphere (see also Figure S6).

Canopy waters of the P508A variant

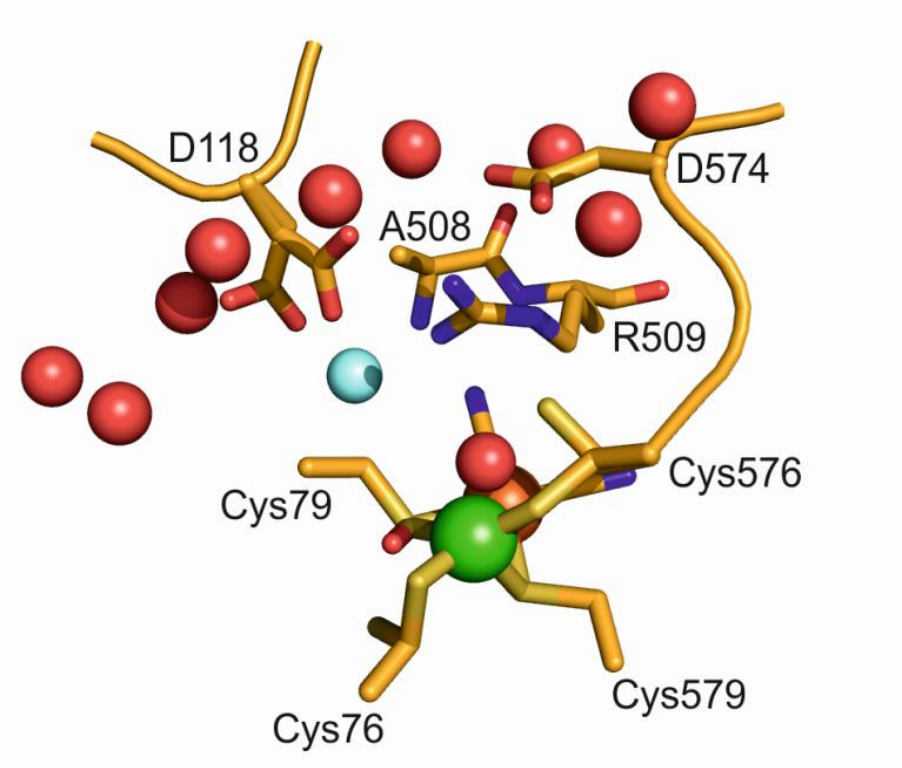

Figure S6: Water structure within the catalytic center of the P508A variant. There are nine highly ordered water molecules (red spheres) within a 9 Å radius of the guanidinium head group of R509 present in the P508A variant that are also present in native Hyd-1 and other canopy variants.(*1*) The change in shape and size of residue 508 in P508A allows an additional water molecule to enter the active site (cyan sphere).

Determination of the pH optima for native Hyd-1 and canopy variants

In order to ensure that solution assay measurements were carried out close to optimal pH conditions in all cases, the pH dependence of activity for each variant was determined electrochemically from the catalytic H_2 oxidation current at 0 V (−0.1 V for D118N/D574N and D574N). A single electrode modified with a film of enzyme was transferred from a H_2-saturated buffer solution at pH 6.0 to other H_2-saturated solutions over the pH range 3.0–9.0, returning periodically to pH 6.0 to correct for any film loss.(*3*) All enzymes showed a similar trend for activity (normalized current) reflecting the change in driving force for H_2 oxidation with pH and the increased formation of Ni-B with increasing pH. The optimal pH, where activity is maximal, differs between the variants (Figure S7) but activity is still >80% for all variants at pH 6.0.

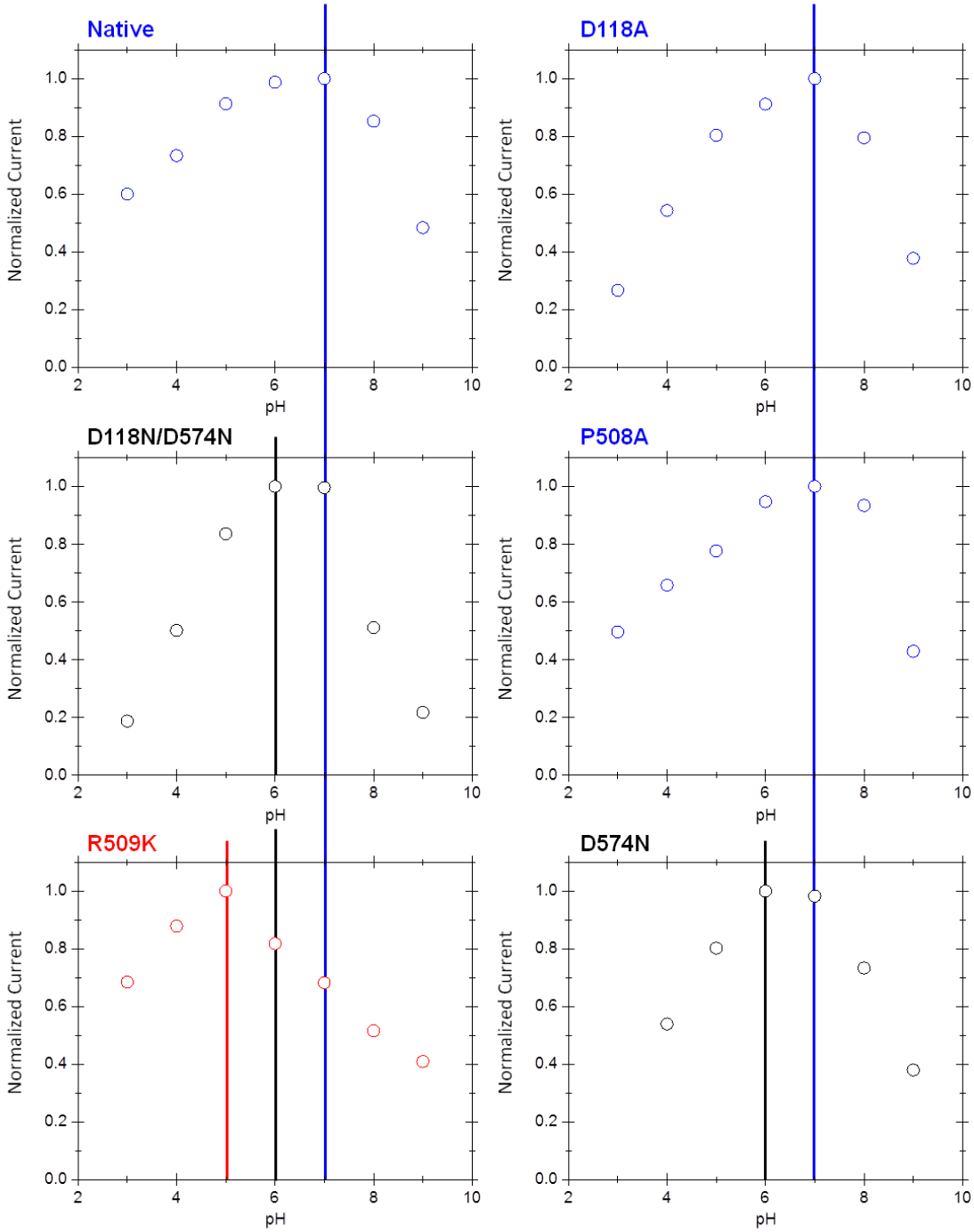

Figure S7: Determination of the pH optima for native Hyd-1 and canopy variants. Chronoamperometry experiments at 0 V (–0.1 V for D118N/D574N and D574N, see text) were performed in 100% H_2. Initially the cell buffer solution was pH 6.0 and once the current had stabilized it was exchanged for different pH buffers in the range pH 3.0-9.0. The buffer was returned to pH 6 periodically to allow for film loss correction. The current at each pH was then normalized to the highest current. Other conditions: 30 ^{o}C, ω = 1000 rpm, total gas flow = 500 scc min^{-1}

Electrocatalytic profiles of native Hyd-1 and canopy variants

The electrocatalytic window of H_2 oxidation for each variant was produced as follows: the enzyme film was exhaustively inactivated at high potential (+0.391 V) and pH 9 under an atmosphere of Ar for 10 000 s; the potential was then scanned from high to low potential at a very slow scan rate (0.1 mVs^{-1}).

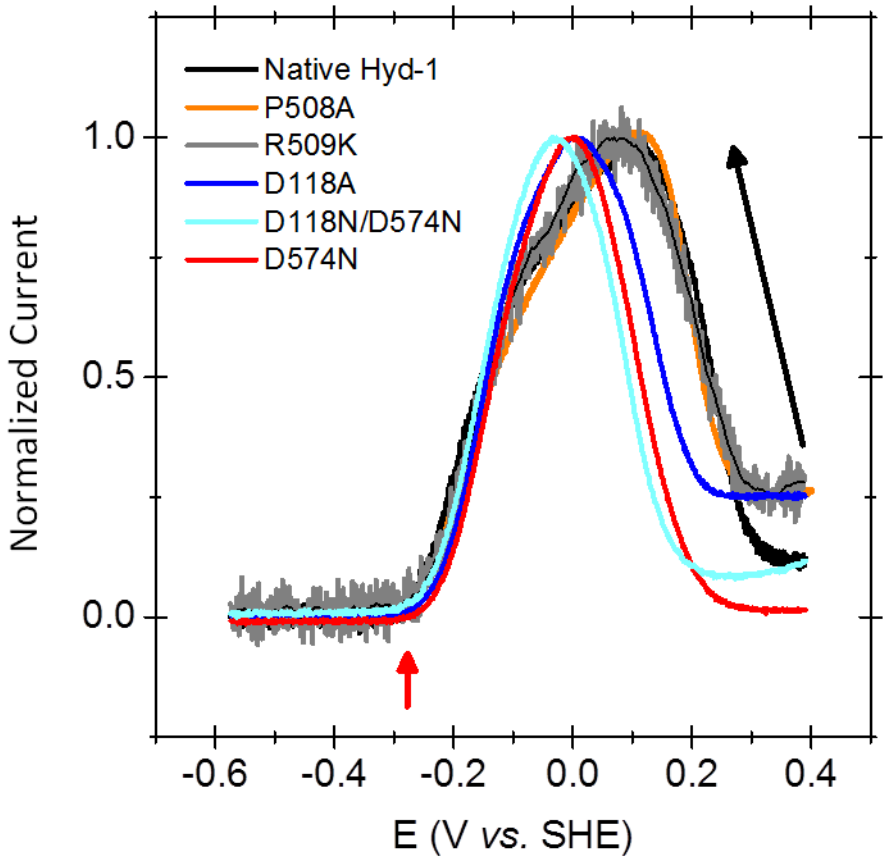

Figure S8: Protein film electrochemistry of native Hyd-1 and the canopy variants. Electrocatalytic profile of Hyd-1 enzymes were produced by linear sweep voltammetry scanning from +0.39 to –0.60 V (black arrow) at a scan rate of 0.1 mVs^{-1} following anaerobic inactivation of the enzyme film as previously described.(*1*) The voltammograms were normalized with respect to the maximum current to allow for comparison of shape and potential markers, rather than current amplitude which varies depending on film quality and history. All enzymes show the same onset potential for hydrogen oxidation (red arrow) but the potential at which the maximum current occurs shifts to more negative potentials as D118 and D574 are changed to neutral residues. All experiments were performed at pH 6, 30 °C, ω = 3000 rpm, 100% H_2, total gas flow rate = 1000 scc min^{-1}

Example Eyring plots for native Hyd-1, D118A and R509K

Eyring plots for Hyd-1, D118A and R509K are shown below. In addition to the 'standard' Eyring plots, the hypothesis that the substitution of proline with alanine would result in the de-stabilization of the protein was investigated by extending the temperature range used: cyclic voltammograms were scanned between –0.66 and +0.24 V at a scan rate of 5 mV s^{-1} between 10 and 65 ^{o}C. The temperature was returned to 30 ^{o}C at regular intervals to allow for film loss correction.(*3*) All the resulting Eyring plots (not shown) were linear, similar to native Hyd-1, showing that P508A did not exhibit a reduction in thermal stability within the temperature range used to determine activation enthalpies.

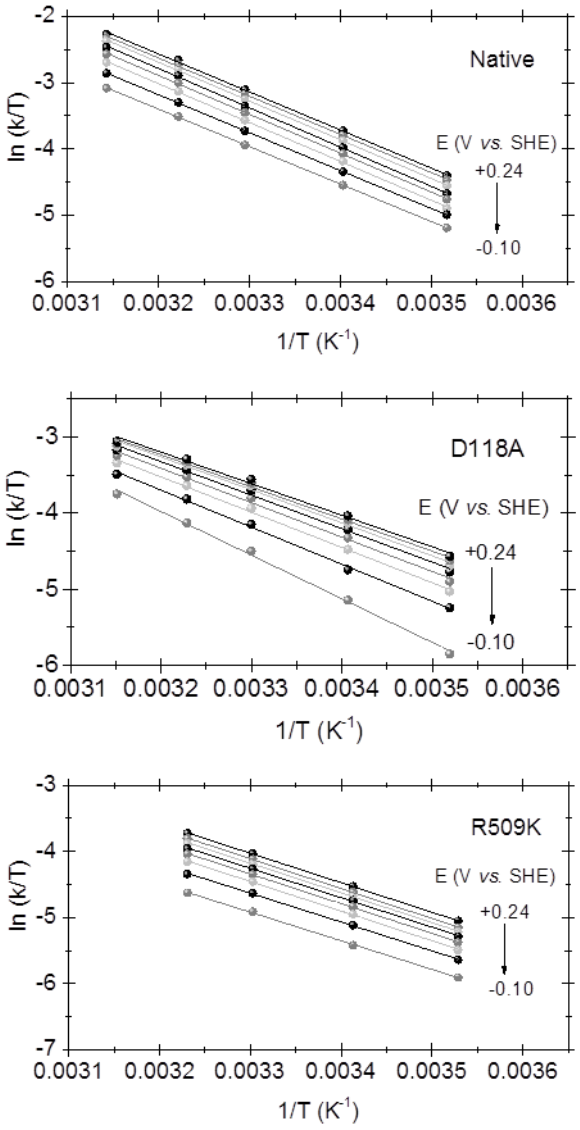

Figure S9: Example Eyring plots for native Hyd-1, D118A and R509K. Cyclic voltammograms were measured at different temperatures in the range 10-45 ^{o}C (internal electrochemical cell temperature) at a scan rate of 5 mVs^{-1} and the current at different potentials was used for Eyring analysis. Cyclic voltammograms at 30 ^{o}C and a scan rate of 30 mVs^{-1} were performed periodically to allow for film loss correction. Other conditions: pH 6, ω = 1000 rpm, 100 % H_2 with a total gas flow rate = 500 scc min^{-1}.

Determination of the activation entropy difference ($\Delta\Delta S^{\ddagger}$) between native Hyd-1 and R509K

The difference in the entropy of activation of native Hyd-1 ($\Delta S_1^{\ddagger}$) and R509K ($\Delta S_2^{\ddagger}$) was calculated from the ratio of the turnover rates (k_1 and k_2, respectively) determined by conventional solution assay, and the enthalpies of activation ($\Delta H_1^{\ddagger}$and $\Delta H_2^{\ddagger}$, respectively) determined by PFE (Table 1):

$$\ln\left(\frac{k_1}{k_2}\right) = \ln(k_1) - \ln(k_2) = -\frac{\Delta H_1^{\ddagger}}{RT} + \frac{\Delta S_1^{\ddagger}}{R} + \frac{\Delta H_2^{\ddagger}}{RT} - \frac{\Delta S_2^{\ddagger}}{R} = \frac{\left(\Delta H_2^{\ddagger} - \Delta H_1^{\ddagger}\right)}{RT} + \frac{\left(\Delta S_1^{\ddagger} - \Delta S_2^{\ddagger}\right)}{R} = 4.4$$

multiplying through by R and T gives:

$$\left(\Delta H_2^{\ddagger} - \Delta H_1^{\ddagger}\right) + T\left(\Delta S_1^{\ddagger} - \Delta S_2^{\ddagger}\right) = 4.4\ RT$$

this rearranges to give:

$$\left(\Delta S_1^{\ddagger} - \Delta S_2^{\ddagger}\right) = \frac{(4.4\ RT) - \left(\Delta H_2^{\ddagger} - \Delta H_1^{\ddagger}\right)}{T} = \frac{10971 + 4828}{303} = 52\ \text{J K}^{-1}\text{mol}^{-1}$$

The value for $\Delta\Delta S^{\ddagger}$ can also be found by calculating the entropy of activation for native Hyd-1 ($\Delta S_1^{\ddagger}$):

$$\Delta S_1^{\ddagger} = R\left(\ln k_1 - \left(\frac{lnk_{\mathrm{B}}T}{h}\right) + \left(\frac{\Delta H_1^{\ddagger}}{RT}\right)\right)$$

$$\Delta S_1^{\ddagger} = 8.314\left(5.55 - (29.5) + (17.7)\right) = -51.4\ \text{J K}^{-1}\text{mol}^{-1}$$

and for R509K ($\Delta S_2^{\ddagger}$):

$$\Delta S_2^{\ddagger} = R\left(\ln k_2 - \left(\frac{lnk_{\mathrm{B}}T}{h}\right) + \left(\frac{\Delta H_2^{\ddagger}}{RT}\right)\right)$$

$$\Delta S_2^{\ddagger} = 8.314\left(1.19 - (29.5) + (15.8)\right) = -103.5\ \text{J K}^{-1}\text{mol}^{-1}$$

The difference in the entropy of activation between native Hyd-1 and R509K is then:

$$\Delta S_1^{\ddagger} - \Delta S_2^{\ddagger} = -51.4 + 103.5 = 52\ \text{J K}^{-1}\text{mol}^{-1}$$

Transient Oxygen Exposure experiments: O_2 injections

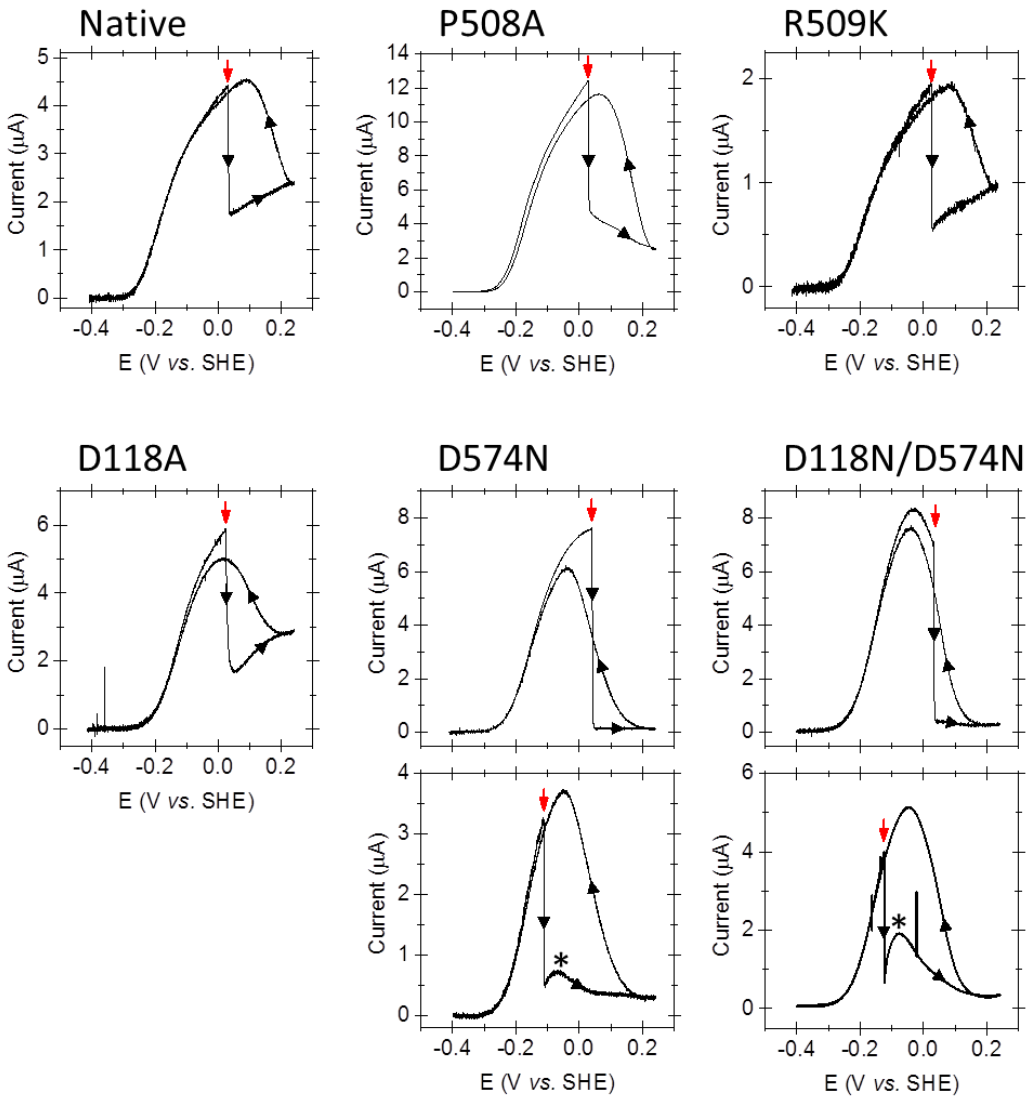

Figure S10: Effect of transient exposure to oxygen on the H_2 oxidation activity for Native Hyd-1 and canopy variants. Under a constant headspace gas of 100% H_2, cyclic voltammograms were performed between –0.40 and +0.24 V at a scan rate of 0.5 mV s^{-1}. For all enzymes, O_2-saturated buffer was injected (red arrow) at +0.03 V to give a total O_2 concentration of 154 μM (upper panels). The constant H_2 flow into the cell headspace and slow scan rate ensured all O_2 is flushed from the system by the time the reverse scan begins. For D118N/D574N and D574N, the experiment was repeated with O_2-saturated buffer injection at a more reducing potential, –0.125 and –0.113 V respectively (lower panels), to compensate for the differences in E_{switch} (Figure S8). Under these adjusted conditions, following the O_2 injection, the H_2 oxidation current for D118N/D574N and D574N begins to increase before anaerobic inactivation occurs at high potential (marked by *). All experiments were performed at pH 6 and 30 ^{o}C, ω = 3000 rpm, total gas flow rate = 1000 scc min^{-1}

Native at 0 V

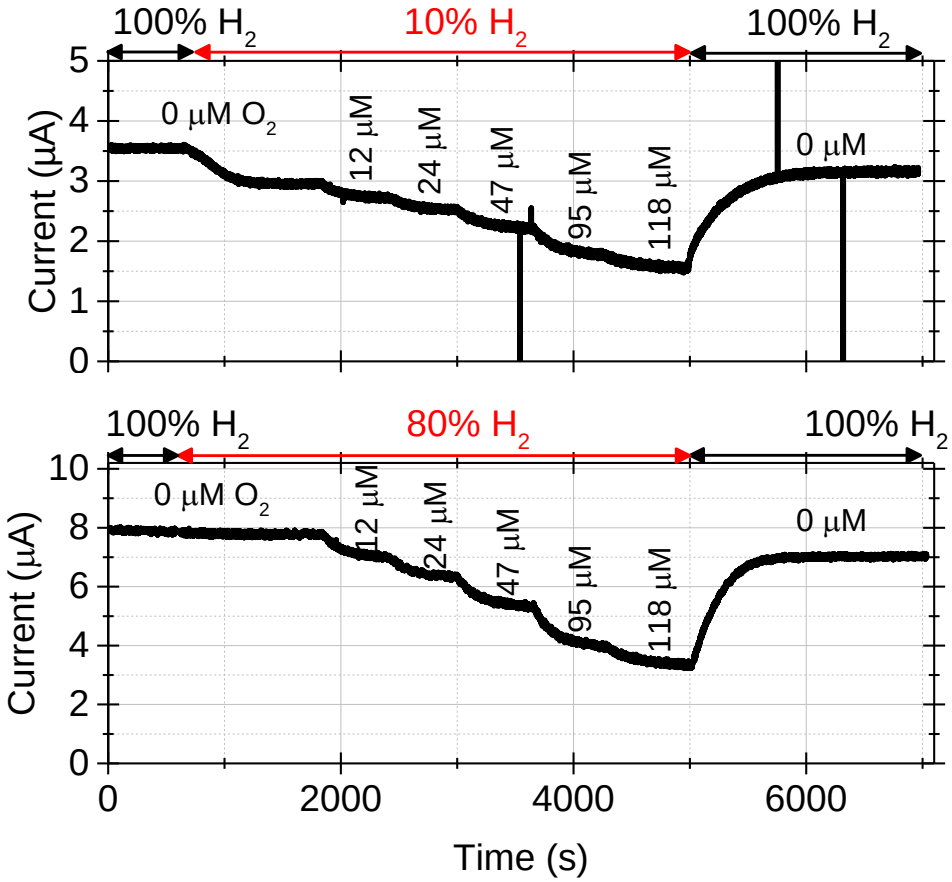

D118A at 0 V

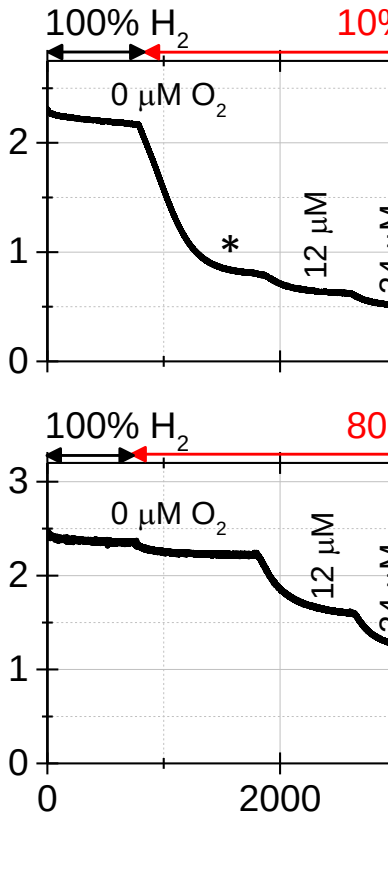

R509K at 0 V

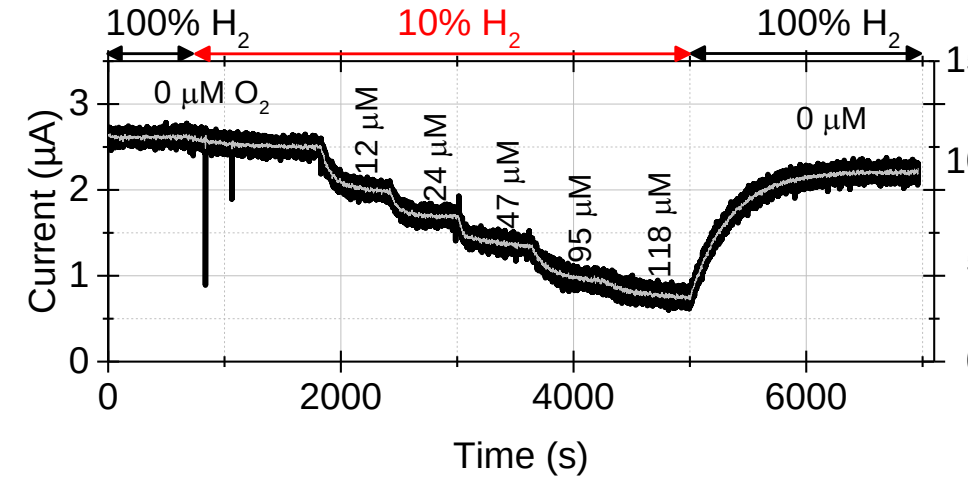

P508A at 0 V

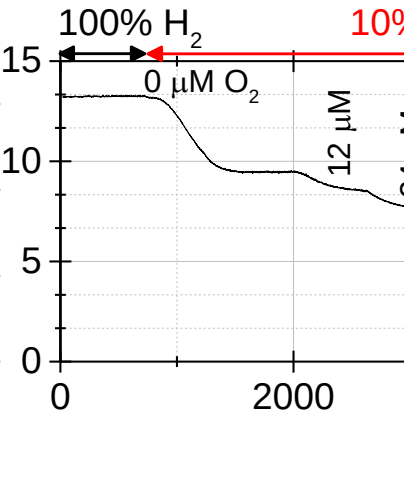

D574N at 0 V

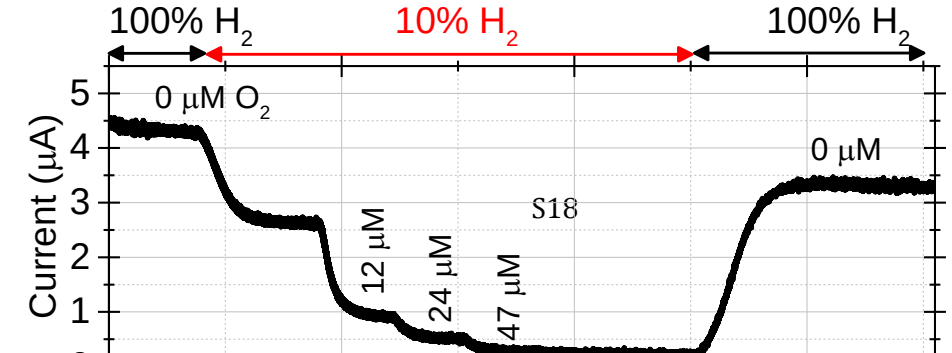

D118N/D574N at 0

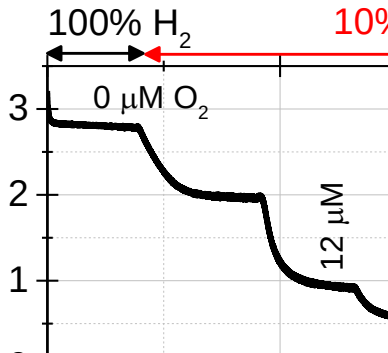

Figure S11: Effect of continuous exposure to oxygen on the H_2 oxidation activity for native Hyd-1 and canopy variants Chronoamperometry experiments measured the current at 0 V in 100% H_2 for the first 700 s before stepping to 10% H_2. After 1100 s, O_2 was added to the headspace and the concentration increased at successive 600 s intervals until all H_2 oxidation current was lost or 10% O_2 was reached. After 5000 s, the O_2 flow was stopped and the headspace gas returned to 100% H_2. After 2000 s at 100% H_2, the enzyme films were held at low potential and the current response at 0 V monitored to determine if any reactivation occurred (not shown). The same experiment was repeated at a more reducing potential for Ni-B reactivation for D118N/D574N and D574N (–0.125 and –0.113 V respectively) to account for differences in E_{switch} (Figure S8). It was also repeated at 80% H_2 for D118A to account for the high $K_M^{H_2}$ (note, as expected, there is a significant drop in H_2 oxidation current when the headspace gas is changed to 10% H_2, as indicated by *). Conditions: pH 6, 30 °C, ω = 3000 rpm, carrier gas = Ar, total gas flow rate = 1000 scc min^{-1}

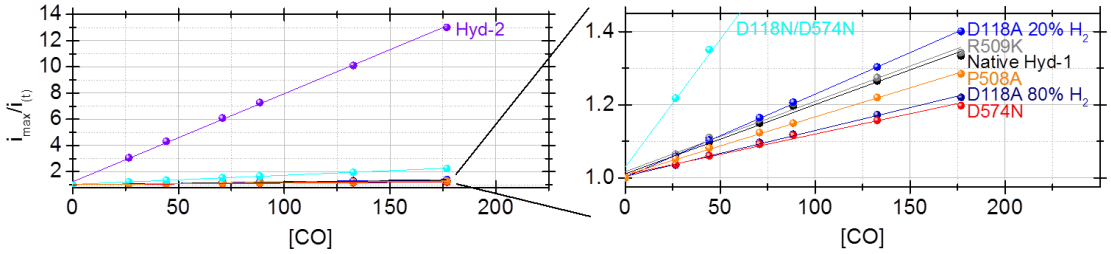

Figure S12: Effect of continuous exposure to CO on the H_2 oxidation activity for Native Hyd-1 and canopy variants. The left panel shows a comparison of Hyd-1with the O_2-sensitive hydrogenase Hyd-2 from *E. coli*, while the right panel shows an enlargement of the Hyd-1 data comparing native and canopy variants. Chronoamperometry experiments were used to measure the current at –0.06 V in 20% H_2 as previously described.(*4*, *5*) After 700 s, CO was added to the headspace and the concentration increased at successive intervals until 20% CO was reached whilst maintaining 20% H_2. After 6200 s, the CO flow was stopped and the headspace returned to 20% H_2. The experiment was repeated in 80% H_2 for D118A to account for the high $K_M^{H_2}$. Conditions: pH 6, 30 °C, ω = 3000 rpm carrier gas = Ar, total gas flow rate = 500 scc min^{-1}

Current offset adjustment for H_2 evolution by R509K

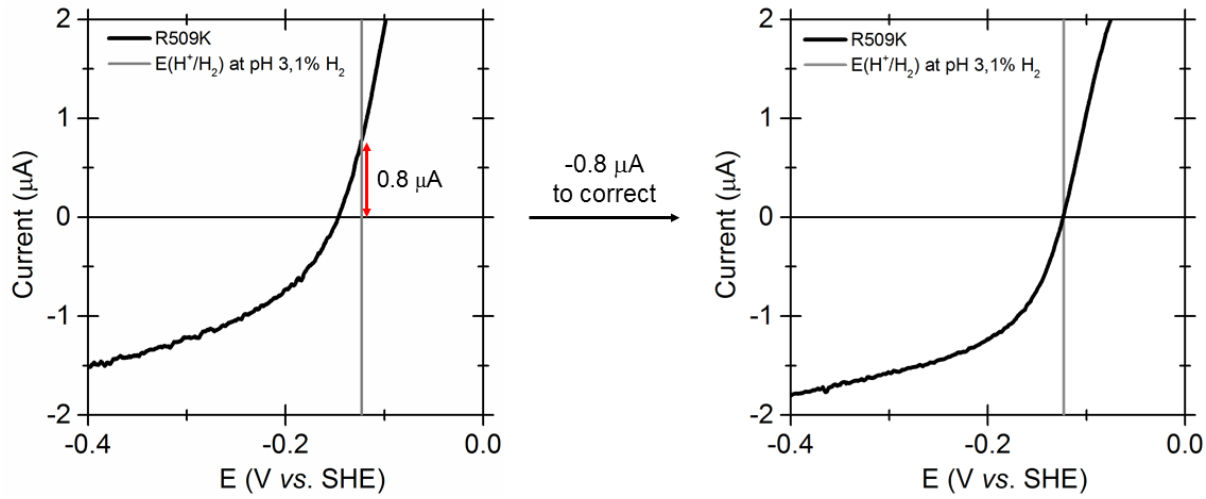

Figure S13: Method of current offset adjustment for R509K. The potential was cycled between –0.45 and +0.05 V at a scan rate of 1 mVs^{-1}. For R509K, a modified electrode was required to produce an appreciable current at pH 3.0 and 1% H_2. The current at each potential was averaged to eliminate the capacitive (non-Faradaic) current. The current at the Nernst potential was then subtracted from the current at each potential so that the voltammogram crossed the zero-current axis at the thermodynamically correct potential as is seen in native Hyd-1 and the other variants. Conditions = 37 ^{o}C, ω = 3000 rpm, carrier gas = Ar, total gas flow rate = 1000 scc min^{-1}

Supplementary Information References

1. Evans, R. M., Brooke, E. J., Wehlin, S. A. M., Nomerotskaia, E., Sargent, F., Carr, S. B., Phillips, S. E. V., and Armstrong, F. A. (2016) Mechanism of hydrogen activation by [NiFe] hydrogenases, *Nat. Chem. Biol. 12*, 46-50.
2. Greening, C., Biswas, A., Carere, C. R., Jackson, C. J., Taylor, M. C., Stott, M. B., Cook, G. M., and Morales, S. E. (2015) Genomic and metagenomic surveys of hydrogenase distribution indicate H_2 is a widely utilised energy source for microbial growth and survival, *ISME J. 10*, 1-17.
3. Evans, R. M., and Armstrong, F. A. (2014) Electrochemistry of Metalloproteins: Protein Film Electrochemistry for the Study of *E. coli* [NiFe]-Hydrogenase-1, in *Metalloproteins - Methods and Protocols* (Fontecilla-Camps, J. C., and Nicolet, Y., Eds.), pp 73-94, Humana Press, New York.
4. Evans, R. M., Parkin, A., Roessler, M. M., Murphy, B. J., Adamson, H., Lukey, M. J., Sargent, F., Volbeda, A., Fontecilla-Camps, J. C., and Armstrong, F. A. (2013) The principles of sustained enzymatic hydrogen oxidation in the presence of oxygen – the crucial influence of high potential Fe-S clusters in the electron relay of [NiFe]-hydrogenases., *J. Am. Chem. Soc. 135*, 2694-2707.
5. Lukey, M. J., Parkin, A., Roessler, M. M., Murphy, B. J., Harmer, J., Palmer, T., Sargent, F., and Armstrong, F. A. (2010) How *Escherichia coli* is equipped to oxidize hydrogen under different redox conditions, *J. Biol. Chem. 285*, 3928-3938.